Fabrication and *ex vivo* evaluation of activated carbon–Pt microparticle based glutamate biosensor

Tran N.H. Nguyen [a], James K. Nolan [a], Xi Cheng [b], Hyunsu Park [a], Yi Wang [a], Stephanie Lam [a], Hyungwoo Lee [c], Sang Joon Kim [c], Riyi Shi [d], Alexander A. Chubykin [b], Hyowon Lee [a,*]

[a] Weldon School of Biomedical Engineering, Birck Nanotechnology Center, Center for Implantable Device, Purdue University, West Lafayette, IN, USA
[b] Department of Biological Sciences, Purdue Institute for Integrative Neuroscience, Purdue University, West Lafayette, IN, USA
[c] Samsung Advanced Institute of Technology, Suwon, South Korea
[d] College of Veterinary Medicine, Purdue University, West Lafayette, IN, USA

ARTICLE INFO

ABSTRACT

As one of the most abundant neurotransmitters in the brain and the spinal cord, glutamate plays many important roles in the nervous system. Precise information about the level of glutamate in the extracellular space of living brain tissue may provide new insights on fundamental understanding of the role of glutamate in neurological disorders as well as neurophysiological phenomena. Electrochemical sensor has emerged as a promising solution that can satisfy the requirement for highly reliable and continuous monitoring method with good spatiotemporal resolution for characterization of extracellular glutamate concentration. Recently, we published a method to create a simple printable glutamate biosensor using platinum nanoparticles. In this work, we introduce an even simpler and lower cost conductive polymer composite using commercially available activated carbon with platinum microparticles to easily fabricate highly sensitive glutamate biosensor using direct ink writing method. The fabricated biosensors are functionality superior than previously reported with the sensitivity of 5.73 ± 0.078 nA μM^{-1} mm^{-2}, detection limit of 0.03 μM, response time less than or equal to 1 s, and a linear range from 1 μM up to 925 μM. In this study, we utilize astrocyte cell culture to demonstrate our biosensor's ability to monitor glutamate uptake process. We also demonstrate direct measurement of glutamate release from optogenetic stimulation in mouse primary visual cortex (V1) brain slices.

© 2020 Elsevier B.V. All rights reserved.

1. Introduction

Glutamate or glutamic acid is one of the primary excitatory neurotransmitters in the nervous system. Its role in long-term potentiation, which is essential in learning and memory, is well recognized [1]. Moreover, glutamate plays a significant role in maintaining and regulating bioenergetic process [2]. Thus, any disruption that results in an abnormal level of glutamate can have significant neurological impact. In normal physiological process, glutamate is released from glutamatergic nerve terminals to be taken up at the target neuron's receptors [3]. The extracellular glutamate concentration is in the order of ~1 μM but can rise up to ~1 mM during action potential [4,5]. In a diseased state such as spinal cord injury, the extracellular glutamate concentration is also thought to be elevated due to glutamate excitotoxicity [6]. Therefore, a better understanding of these dynamic extracellular glutamate levels can have a tremendous impact on basic neuroscience and neurodegeneration research.

There are several existing methods to quantify glutamate concentration *in vivo* including positron emission tomography, magnetic resonance spectroscopy, and microdialysis [7]. However, they have poor spatiotemporal resolution that limits their utility given rapid transient behavior of extracellular glutamate [8]. Enzymatic electrochemical biosensors can provide a superior temporal resolution for measuring levels of glutamate *in vivo* [9,10]. Table 1 presents a brief comparison of existing methods for *in vivo* measurement of glutamate.

In the literature, there are several examples of first-generation oxidase-based biosensors for amperometric detection of glutamate *via* H_2O_2 oxidation [11–13]. In the presence of oxygen, glutamate oxidase (GluOx) catalyzes glutamate to form H_2O_2 (R1) that can be oxidized at the electrode surface as shown below (R2).

$$L-glutamate + H_2O + O_2 \rightarrow alpha-ketoglutarate + NH_3 + H_2O_2 \tag{1}$$

$$H_2O_2 \rightarrow O_2 + 2H^+ + 2e^- \tag{2}$$

Coupled with microelectromechanical systems (MEMS) fabrication techniques, there are now a number of microscale enzymatic glutamate

* Corresponding author.
E-mail address: hwlee@purdue.edu. (H. Lee).

Table 1
Different methods for *in vivo* measurement of glutamate.

Method	Temporal resolution	Spatial resolution	Detection limit	Additional quantification method/requirement	Reference
Microdialysis	>Minutes	$\geq 0.6\ mm^2$	~1 μM	High performance liquid chromatography	[7,40,41]
Nuclear magnetic resonance spectroscopy	>Minutes	mm^3 (non-invasive)	~mM	Large equipment	[42,43]
Positron emission tomography	Seconds to minutes	mm^3 (non-invasive)	<1 μM	Large equipment	[44,45]
Optical sensors	ms	<100 nm	<1 nM	Optical access	[46,47]
Electrochemical microsensor	≤1 s	<100 μm	<0.1 μM	N/A	[37,48,49]

electrochemical biosensors that can also provide superior spatial resolution than previously possible [14–16]. Although these MEMS-fabricated electrochemical biosensors perform well *in vitro* and *in vivo*, they are often difficult and expensive to fabricate. Since they often require photomasks to manufacture a fixed design, it is also difficult to make changes to sensor geometries. With advances in additive manufacturing, there are now more flexible fabrication techniques to allow for rapid iteration between biosensors designs [17]. We recently published a simple direct ink writing (DIW) method to fabricate glutamate biosensors for *in vivo* application [18].

In this work, we introduce an even more economical yet functionally superior composite material for biosensor fabrication based on commercially available activated carbon with Pt microparticles (CPt). A preliminary version of this work has been reported in 2018 IEEE Sensors Conference [19]. Here we optimized the sensor performance to demonstrate that the CPt based glutamate biosensors have a superior performance compared to the MEMS-fabricated and the Pt nanoparticle-based glutamate biosensors [18]. CPt was mixed with a well-known conductive polymer, poly (3,4 ethylenedioxythiophene): poly (styrenesulfonate) (PEDOT:PSS), to create a dispensable composite ink that can be printed on any soft or hard substrate including polydimethylsiloxane (PDMS) and liquid crystal polymer (LCP). The new CPt glutamate biosensors have better sensitivity, limit of detection, response time, linear range, and stability compared to our previous Pt nanoparticle-based version. Using an astrocyte cell culture, we demonstrate the capability to monitor extracellular glutamate consumption. Additionally, we present a direct *ex vivo* measurement of glutamate release from optogenetic stimulation in mouse primary visual cortex (V1) brain slices.

2. Methods

2.1. Reagents

Ascorbic acid (AA), acetaminophen (AC), and uric acid (UA) were purchased from Alfa Aesar (Thermo Fisher Scientific, Waltham, MA). Glutamate oxidase (GluOx) from Streptomyces was purchased from Cosmo Bio USA (Carlsbad, CA) with a rated activity of 25 units/mg of protein. PEDOT:PSS (5 wt%), Nafion® 117 solution (5 wt%), 3,4-Dihydroxyphenylacetic acid (DOPAC) and 5-hydroxyindoleacetic acid (5-HIAA) were purchased from Sigma Aldrich (St. Louis, MO). Bovine serum albumin (BSA, >96%), hydrogen peroxide (30%), glutaraldehyde (25% in deionized water), L-glutamic acid, dimethyl sulfoxide (DMSO), 0.1 M phosphate buffer solution (PBS, pH 7.0), C-PT paste (10% Pt) were purchased from Fisher Scientific (Waltham, MA). Ag/AgCl (CI-4001), Ag (CI-1001) and were purchased from Engineered Conductive Materials Inc. (Delaware, OH). Carboxylic functionalized multi-walled carbon nanotube (MWCNT) was purchased from Cheap Tubes Inc. (Grafton, Vermont). Ag/AgCl/NaCl (3.5 M) reference electrode for astrocyte measurement was purchased from (Bio-logic USA, LLC, Knoxville, TN, USA). Human cerebral cortex astrocytes, astrocyte medium and cell freezing medium were obtained from ScienCell Research Laboratories (Carlsbad, CA). Astrocyte medium consisted of 500 ml of basal medium, 10 ml of fetal bovine serum (FBS, Cat. No. 0010), 5 ml of penicillin/streptomycin solution (P/S, Cat. No. 0503), and 5 ml of astrocyte growth supplement (AGS, Cat. No. 1852).

2.2. Ink preparation

Two different composite inks were used to complete the fabrication of the new glutamate biosensors. The first ink formulation was for the working and the counter electrodes. It was prepared by modifying conductive polymer (PEDOT:PSS) with CPt. The polymer composite consisted 1 wt% of Pt, which was constructed by mixing 100 mg of CPt paste and 400 mg of PEDOT: PSS in a planetary centrifugal mixer (ARE-310, Thinky U.S.A., Inc., Laguna Hills, CA) for 30 min and degassing for additional 10 min.

Because C-Pt-modified PEDOT:PSS exhibited high resistance, a second ink was developed to create a more conductive electrical traces. It consisted of PEDOT:PSS modified with 1 wt% of MWCNT and 22 wt% of DMSO to improve its conductivity [20]. Ecoflex (20 wt%) was also added to improve the flexibility of the ink [21]. MWCNT was first mixed with DMSO in sonication bath for 2 h. The mixture then was added to PEDOT:PSS ink and transferred to the planetary centrifugal mixer and mixed for 1 h. Next, Ecoflex was added, and mixed for 10 min. Finally, the composite was degassed using the planetary centrifugal mixer for another 1 h. The final mixture was dried at 60 °C in vacuum for 1 h to remove excess DMSO and to create desired viscosity for printing.

Commercially available Ag (CI-1001, Engineered Materials Solutions, Inc., Delaware, OH) and Ag/AgCl (CI, 4001, Engineered Materials Solutions, Inc., Delaware, OH) pastes were used to print the contact pads and the reference electrodes. Lastly, PDMS was applied as an insulating layer leaving only the electrode areas open.

2.3. Fabrication and direct ink writing process

Fig. 1 shows the construction of our DIW glutamate biosensor. A three-axis automated microfluidic dispensing system (Pro-EV3 and Ultimus V, Nordson EFD, East Providence, RI) was used as the DIW platform that can position the dispensing tip with ±8 μm accuracy within the working space of 400 mm². A pressurize 3 cc syringe barrel (Nordson EFD, East Providence, RI) was used as the ink reservoir. A custom glass capillary pipette with 30 μm-diameter tip was fabricated using micropipette puller (Sutter Instrument, Novato, CA) to dispense the ink. Here, an output pressure ranged from 10 to 40 psi, and the printing speed was varied from 1 to 5 mm/s. The biosensors were printed on either PDMS or LCP (Ultralam 3850, Rogers Corporation, Chandler, AZ, USA) substrate. PDMS was prepared by spin coating PDMS on a glass slide. The glass slide was precoated with 1 μm layer of Parylene C to promote device release. The biosensors were also printed on a 100-μm-thick LCP sheet. To complete the glutamate biosensor with good selectivity, Nafion and glutamate oxidase were deposited using a previously described method [18]. After the enzyme immobilization, the samples were stored in room temperature for 48–72 h, and in 4 °C until testing.

2.4. Biosensor evaluation

A field-emission scanning electron microscopy (FESEM, S-4800, Hitachi, Japan) was used to examine the physical structure and surface morphology of the C-Pt–PEDOT:PSS composite. Cyclic voltammographs (CV) and chronoamperometry measurements were obtained using a conventional three-electrode cell to evaluate the electrochemical characteristics of the fabricated biosensors. A commercial potentiostat (SP-200, Bio-
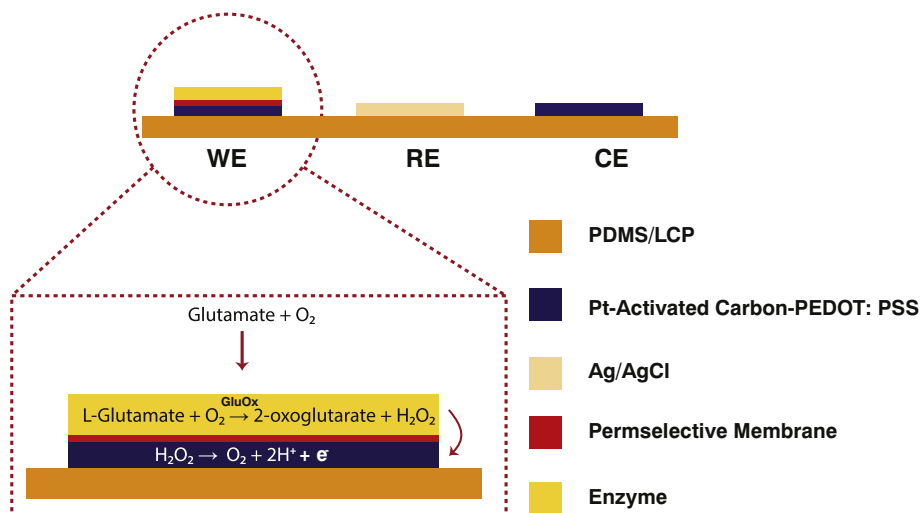
Fig. 1. Cross-sectional view of the C-Pt–PEDOT:PSS based glutamate biosensor. The conventional three-electrode construction allows amperometric measurement of glutamate concentration continuously. Briefly, the glutamate oxidase converts glutamate into H_2O_2, which is then oxidized on the electrode surface to generate current.

logic USA, LLC, Knoxville, TN, USA) was used to perform all electrochemical analysis. All CV measurements were performed in the potential range of -0.6–0.8 V using the scan rate of 100 mV/s and the sampling interval of 1 mV/s. All amperometry data were obtained at 0.5 V *vs.* Ag/AgCl after 20 min of settling time with a 0.3 s sampling interval. The supporting electrolyte solution was 50 ml of 0.01 M PBS (pH 7.0) for all experiments unless stated otherwise. During the amperometry experiments, a stir bar was placed at 180 rpm in the electrolyte solution. A Faraday cage was used to reduce the background noise. The stability of our printed sensors was evaluated by comparing their glutamate sensitivity before and after 3 weeks of storage in 0.01 M PBS (pH 7.0) at 4 °C. Electrochemical impedance spectroscopy (EIS) was performed by delivering 10 mV sinusoid excitation voltage to the working electrode. The magnitude and the phase of electrode impedance were measured from 10 to 100 kHz in 0.01 M PBS (pH 7.0). All current measurements from the amperometry experiments were normalized to the geometric surface area of tested electrodes.

2.5. Cell cultures preparation

Human cerebral cortical astrocytes were obtained from Sciencell (Carlsbad, CA). Astrocytes were cultured to near confluency (until the cells nearly cover culture surface), and then removed from the culture plate using Trypsin-EDTA, centrifuged, and resuspended to $>1 \times 10^6$ cells/mL. They were frozen in a medium containing DMSO in liquid nitrogen. Astrocytes were expanded and maintained per Sciencell's protocol. Astrocytes were cultured in 12-well, tissue culture-treated plates, with 10^5 cells seeded per well. These cultures were then incubated until confluency (~2 d) in a humidified atmosphere with 5% CO_2 at 37 °C. The medium was replaced 1 d after seeding. Prior to the amperometric measurements, the cultures were washed twice with 0.01 M PBS (pH 7.0), and then placed in 1.5 ml of 0.01 M PBS (pH 7.0).

2.6. Glutamate consumption measurement

Prior of each recording measurement, glutamate sensors were calibrated in 0.01 M PBS (pH 7.0) electrolyte solution to determine their baseline sensitivity. For glutamate consumption measurement, the glutamate biosensor, Ag/AgCl reference electrode, and Pt-wire counter electrode were placed in the culture well with astrocytes and 1.5 ml of 0.01 M PBS (pH 7.0). The glutamate biosensor was oriented perpendicular to the cell culture well surface. The glutamate biosensor was then lowered until its tip touched the cell culture well surface, so the sensor electrode was ~100 μm away. We applied 0.5 V *versus* reference to the glutamate sensor and waited 20 min for the non-faradaic current to settle. Then, we added

0.5 ml of 0.9 mM glutamate ($n = 3$), resulting in a final concentration of 225 μM in 2 ml of 0.01 M PBS (pH 7.0). As a control, this same procedure was repeated in wells without cells ($n = 3$).

2.7. Animal and acute brain slice experiments

All animal experiments were reviewed and approved by the Purdue University Animal Care and Use Committee. Brain slices preparation was followed as in previous study [22]. Male B6.Cg-Tg (Thy1-COP4/EYFP) 18Gfng/J (Thy1-ChR2-YFP) mice of 3–4 months old from Jackson Lab were anesthetized by intraperitoneal injection with a mix of 90 mg/kg ketamine and 10 mg/kg xylazine. *Trans*-cardiac perfusion was carried out with oxygenated (carbogen from Airgas: 95% O_2, 5% CO_2) choline chloride artificial cerebrospinal fluid (choline chloride ACSF, composition in mM: 1.25 NaH_2PO_4, 25 $NaHCO_3$, 110 choline chloride, 10 dextrose, 2.5 KCl, 0.5 $CaCl_2$, 7 $MgCl_2$, 3.1 pyruvic acid, 11.6 ascorbic acid). The brain was dissected immediately after finishing perfusion. Once collected, the brain was shaped and fixed in the cutting chamber of the vibratome (Leica VT1000), which was filled with the ice-cold choline chloride ACSF and oxygenated continuously with carbogen flow. Three hundred micrometer thick coronal brain slices containing the visual cortex were collected and placed immediately to a 32 °C incubation chamber with oxygenated ACSF (composition in mM: 1.25 NaH_2PO_4, 26 $NaHCO_3$, 10 dextrose, 124 NaCl, 2.5 KCl, 2 $CaCl_2$, 0.8 $MgCl_2$) for at least 30 min. The brain slices were then placed at room temperature (25 °C) for at least 1 h before use.

2.8. Optogenetic stimulation of brain slices

The Thy1-ChR2-YFP line 18 mice express a light-gated cations channel protein, channelrhodopsin-2 (ChR2) in the Layer 5 pyramidal neurons of visual cortex [23]. During the experiment, oxygenated ACSF was perfused over the slice at ~1 ml/min. The working electrode was placed on the experiment platform underneath the brain slice for direct contact. Ag/AgCl and Pt wire functioned as reference and counter electrode, respectively. The slice was kept in place by a slice hold-down to prevent movement of slice during the experiment. The focal blue light of 470 nm was shed on the layer 5 of the visual cortex of the brain slice through the objective lens of the microscope, which would stimulate influx of cations through ChR2 to depolarize the neurons. Depolarized presynaptic neurons would release glutamate into synaptic clefts with excess glutamate diffusing to the sensor below the brain slice. The light-emitting diode (LED) source (8.1 mW, Mightex Toronto, Ontario M3A) was controlled through its analog port using BioLED Analog and Digital I/O Control Module from the

same company as the LED source. We applied light stimulation of 20 Hz, 5 ms in width, for 1 s every 15 s (Fig. 7d).

3. Results and discussion

According to literature, PEDOT:PSS exhibits superior electrical conductivity and chemical stability [24], as well as high degree of porosity to allow rapid ionic exchange between material and electrolyte surrounding environment [25]. In this study, a low-cost commercial CPt was utilized to improve the catalytic properties of PEDOT:PSS. Pt is used widely in the construction of many microscale electrochemical biosensors [18,25,26]. Activated carbon is also well-known for its porosity and high surface area that are advantageous as electrocatalytic/adsorbent material for oxidation of H_2O_2 [27–29]. By using a commercially

a.
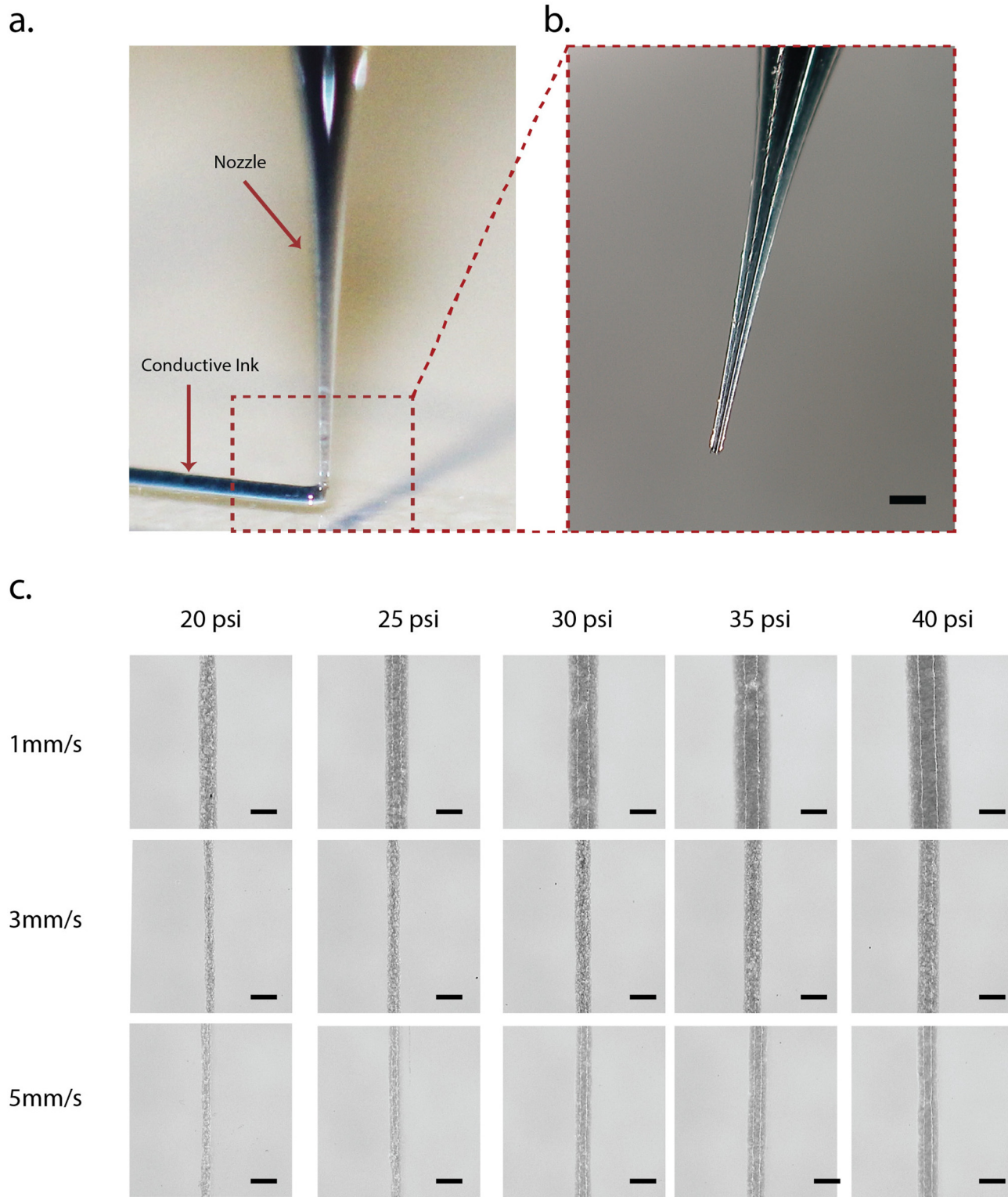
b.

c.

| 20 psi | 25 psi | 30 psi | 35 psi | 40 psi |

Fig. 2. Resolution of our direct ink writing platform. (a–b) Photographs of a custom pulled-pipette dispensed tip (scale bar = 200 μm). (c) Photographs of dispensed of conductive ink at various speeds and pressures (scale bars = 100 μm, SI Table 1).
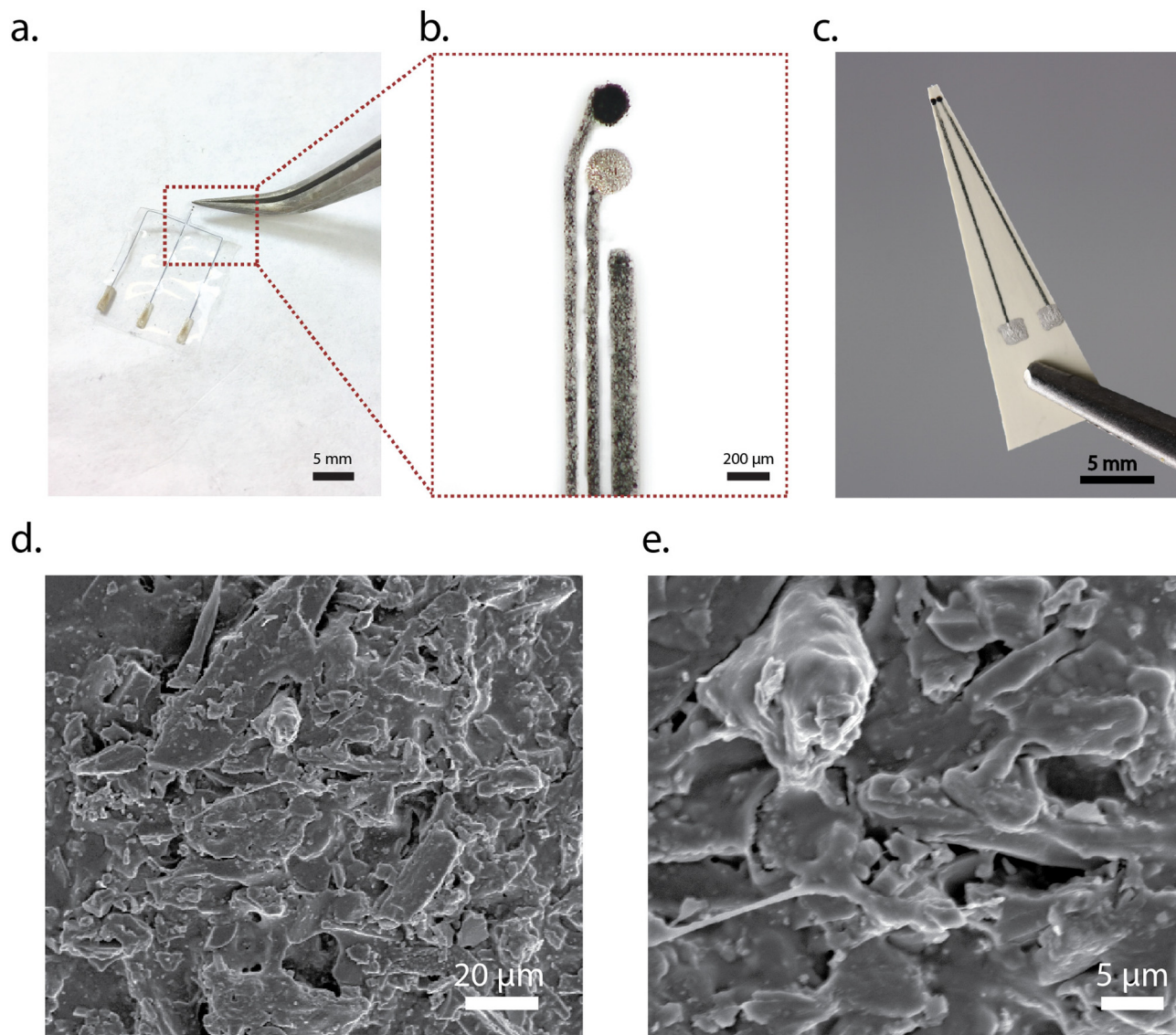
a.

b.

c.

d.

e.

Fig. 3. Printed glutamate biosensor. (a) A photograph of a fully-released glutamate biosensor printed on a PDMS substrate. (b) A close up view of the three electrodes (*i.e.*, working, reference, and counter electrodes). (c) A photograph of a printed glutamate biosensor printed on an LCP substrate for recording with astrocyte cells. (d–e) Scanning electron micrographs of C-Pt–PEDOT:PSS composite at different magnifications.
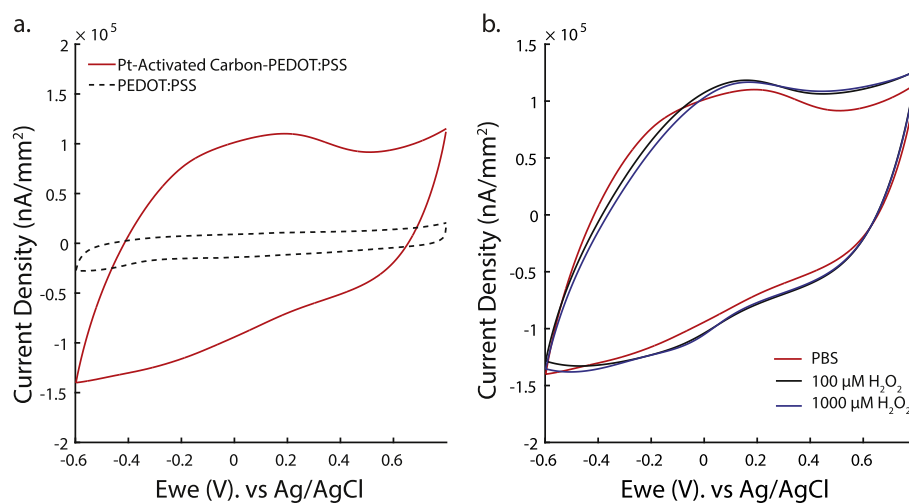

Fig. 4. (a) Cyclic voltammetry of C-Pt–PEDOT:PSS compare to PEDOT:PSS alone in 0.01 M PBS (pH 7.0). Scan rate = 100 mV s^{-1}. Note that the C-Pt–PEDOT:PSS exhibited higher catalytic activity compared to PEDOT:PSS alone. (b) Cyclic voltammetry of C-Pt–PEDOT:PSS composite in 0.01 M PBS (pH 7.0), 100 μ M and 1000 μM H$_2$O$_2$. Scan rate = 100 mV s^{-1}.

available CPt paste, we were able to create a highly sensitive electrode surface upon which to build our enzymatic glutamate biosensors. The resulting conductive ink can be processed using DIW with necessary

flexibility that enabled us to rapidly prototype microscale glutamate biosensors. Fig. 1 shows the schematic of the printed CPt based glutamate biosensor.
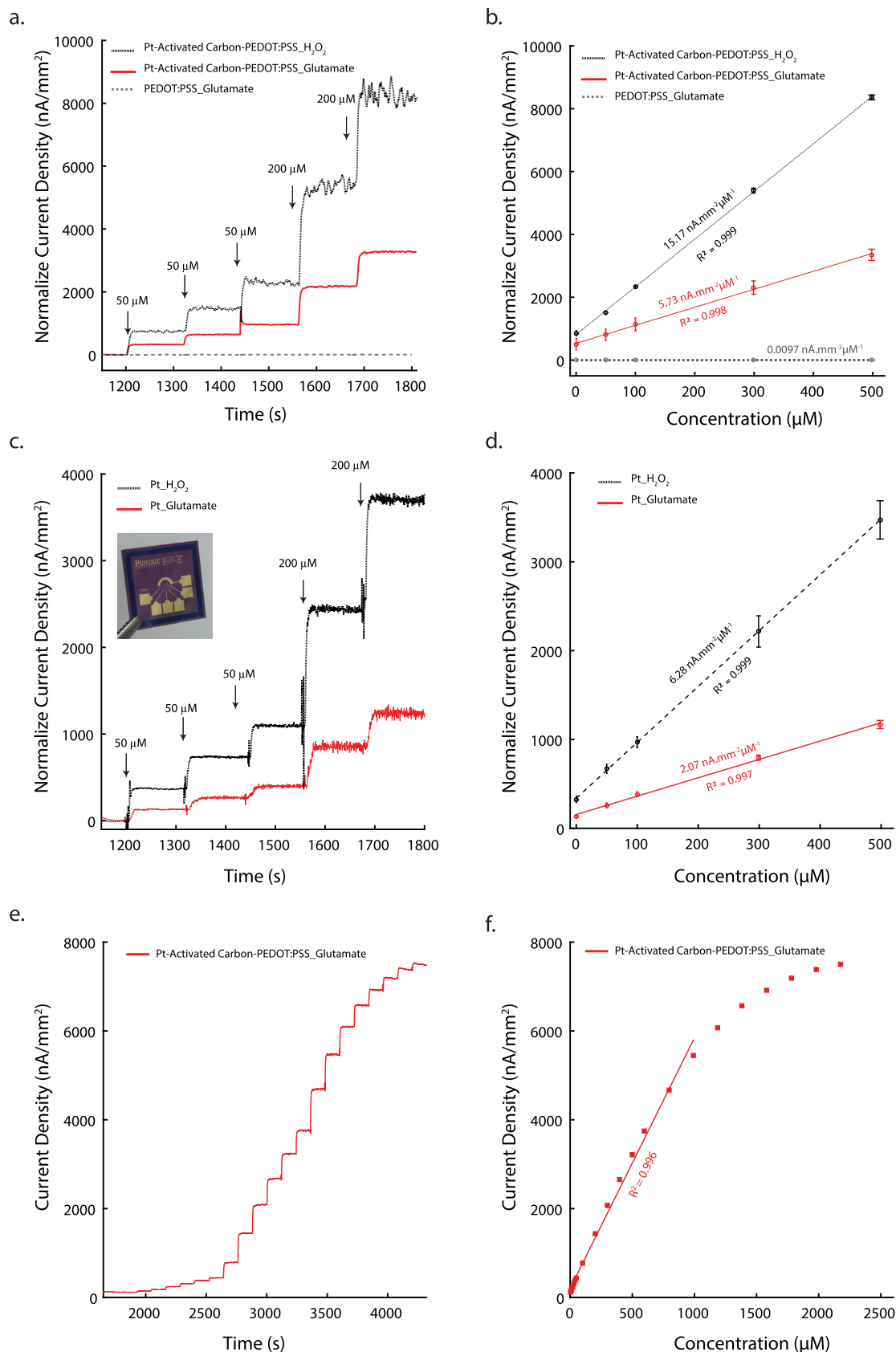
(caption on next page)

Table 2
Different type of glutamate biosensors.

Type of electrode	Fabrication method	Sensitivity (nA μM^{-1} mm^{-2})	Limit of detection (μM)	Response time (s)	Linear range (μM)	Flexibility	Estimated cost	Reference
Pt	Commercial Pt wire	0.85	0.7	2	200	N/A	N/A	[50]
Carbon fiber	Commercial carbon fiber	1.35	< 2	N/A	150	N/A	N/A	[48]
Polyimide base/Pt	MEMS	2.16	0.22	5	150	Flexible (base only)		[37]
Silicon/Pt	MEMS	2.07	0.12	3	N/A	Rigid	$ 57/device	This study
Pt/MWCNT	Electrodeposition	3.84	0.3	7	0–150	Rigid	N/A	[51]
Screen-printed/CNT	Commercial screen-printed	0.057	0.01	5	0.01–10	Rigid	N/A	[52]
Pt-C-PEDOT:PSS	Direct ink writing	5.73	0.03	≤ 1	1–925	Flexible	$ 1.2/device	This study

3.1. Fabrication results and surface characterization

We first characterized the resolution limit of our dispensing process to optimize our printing parameters. The dispensing pressure and the printing speed were varied with ~30-μm-wide custom glass capillary dispensing tip to optimize the line width of the conductive polymer (Fig. 2a–b). Fig. 2c presents the resulting lines with different printing parameters. We were able to print lines as small as 35 μm by applying a higher writing speed with a lower pneumatic pressure (Table S1).

The conductive traces made using C-Pt–PEDOT:PSS ink had high resistance (20–140 kΩ) that prevented us from using the composite (Figs. S1–2). Thus, we modified PEDOT:PSS with MWCNT, which significantly improved the conductivity (Fig. S3). For consistent fabrication of our biosensor, we kept the width of our conductive trace to be ≤100 μm. We also characterized the composites by EIS. EIS measurements (Fig. S4a) showed that the impedance of MWCNT-PEDOT:PSS electrodes was 4.5 orders of magnitude lower than that of C-Pt-PEDOT:PSS electrodes at 1 kHz, which is a commonly used metric for average impedance of electrode [30]. At 1 kHz, the impedances were 2.62 ± 0.88 kΩ and 12.02 ± 0.17 kΩ for MWCNT-PEDOT:PSS and C-Pt-PEDOT:PSS, respectively.

Fig. 3a–b show the printed glutamate biosensors. The diameter of the fabricated sensor surface was about 200 μm. The PDMS-based sensor was approximately 25-μm-thick. The thin-film device was highly compliant upon released and conformed well to the underlying surface, which highlighted the possibility of creating flexible and wearable sensor arrays using this approach [31]. Fig. 3c presents another type of printed biosensor on a 100-μm-thick LCP substrate. This thin-film device was stiff enough to be vertically positioned into a cell culture plate or placed flat underneath brain slices.

Finally, we utilized FESEM to examine the surface morphology of the C-Pt–PEDOT:PSS composite (Fig. 3d–e). We saw that the polymer composite electrodes had rough and porous surface with Pt microparticles embedded in PEDOT:PSS. The rough surfaces have been shown to have greater catalytic activity for H_2O_2, thus corresponding to a higher sensitivity for amperometric oxidase-based biosensors [32]. In addition, the relative rough surface may help improve the response time and lower the limit of detection for enzymatic electrochemical biosensors [32].

3.2. Cyclic voltammetry

Fig. 4a shows the CV of an activated C-Pt–PEDOT:PSS composite compared to PEDOT:PSS alone. An electrode made of PEDOT:PSS exhibited rectangular voltammogram because of its non-Faradaic charging current. It is a product of the conductivity of this polymer material and capacitive behavior between the electrode surface and 0.01 M PBS (pH 7.0) [33]. When PEDOT:PSS was modified with CPt, the voltammogram of electrode exhibited a much higher current density than PEDOT:PSS alone. As such,

the electrochemical response of C-Pt–PEDOT:PSS composite electrode was expected to be superior than PEDOT:PSS electrode alone.

The function of glutamate oxidase biosensor is based on the detection of enzymatically generated H_2O_2. The use of Pt together with carbon materials is known to enhance the detection of H_2O_2 [34,35]. Thus, we examined the electrocatalytic property of the PtC composite using cyclic voltammetry in both buffer and H_2O_2 solutions. Fig. 4b shows the CV of the C-Pt–PEDOT:PSS composite in different concentration of H_2O_2. The C-Pt–PEDOT:PSS electrode exhibited good electrocatalytic activity against H_2O_2, which suggests that these electrodes could serve as a first generation electrochemical platform for detection of glutamate *via* oxidase-based mechanism. Electrochemical behavior of H_2O_2 starts at around 0.1 V and can go up of 0.7 V *vs.* Ag/AgCl in the positive direction. In this case, an oxidation wave starts to display at around 0.2 V with increasing current due to addition of H_2O_2. At 0.5 V, the difference in current between 100 μM and 1000 μM of H_2O_2 is reaching its peak. Therefore, we selected 0.5 V as the potential for glutamate detection.

3.3. Amperometric responses of the glutamate biosensor

Fig. 5a shows the *i-t* responses of C-Pt–PEDOT:PSS composite sensors against H_2O_2 and glutamate. The calibration plot (Fig. 5d) shows that C-Pt–PEDOT:PSS composite had a linear response with a sensitivity of 5.73 ± 0.08 nA μM^{-1} mm^{-2} (n = 3) for glutamate and 15.17 ± 0.12 nA μM^{-1} mm^{-2} for H_2O_2 (n = 3). As a comparison, we also utilized MEMS-fabricated Pt microelectrodes (50-μm-diameter) as glutamate biosensors and characterized their performance. We immobilized glutamate oxidase and Nafion on e-beam evaporated microscale Pt-disc. Fig. 5c–d shows the amperometric responses and the calibration curve of the MEMS glutamate biosensor against H_2O_2 and glutamate. The MEMS biosensor had a sensitivity of 2.07 ± 0.02 nA μM^{-1} mm^{-2} (n = 3) for glutamate and 6.28 nA μM^{-1} mm^{-2} ± 0.51 for H_2O_2 (n = 3).

Additionally, we examined the dynamic range of our printed biosensors with successive addition of glutamate from 1 μM to 2000 μM (Fig. 5e). We found that our C-Pt–PEDOT:PSS composite biosensor exhibited a linear range from 1 μM and 925 μM (R^2 = 0.996) at 0.5 V *vs.* Ag/AgCl (Fig. 5f). The detection limit was 0.03 ± 0.003 μM (n = 3), and the response time ≤ 1 s. Thus, we concluded that our C-Pt-based printed glutamate biosensors have high sensitivity, good linearity, low detection limit and fast response time as comparing to the MEMS biosensor as well as previously reported glutamate biosensors (Table 2).

The printed glutamate biosensors showed 65% higher sensitivity compared to the MEMS-fabricated glutamate biosensor. These results are encouraging because they demonstrate the possibility of fabricating high-quality biosensor using commercially available low-cost materials and direct-writing technology. For small-batch fabrication, this approach would be more economical and efficient than conventional microfabrication techniques. Furthermore, we may be able to increase the

← **Fig. 5.** (a) Representative amperometric curves for C-Pt–PEDOT:PSS and PEDOT:PSS in 0.01 M PBS to glutamate and H_2O_2 (n = 3, each). (b) The corresponding calibration curves and the sensitivity of each glutamate biosensor materials to glutamate and H_2O_2 (n = 3, each). (c) Representative amperometric curves for MEMS–fabricated biosensors in 0.01 M PBS (pH 7.0) to glutamate and H_2O_2 (n = 3, each). Inset: a photograph of a MEMS glutamate biosensor. (d) The corresponding calibration curves and the sensitivity of MEMS–fabricated sensor to glutamate and H_2O_2 (n = 3, each). (e) An amperometric curve of C-Pt–PEDOT:PSS to large range of different concentrations of glutamate in 0.01 M PBS (pH 7.0) solution. (f) The corresponding calibration curve for C-Pt–PEDOT:PSS biosensor to glutamate up to 925 μM (R^2 = 0.996).
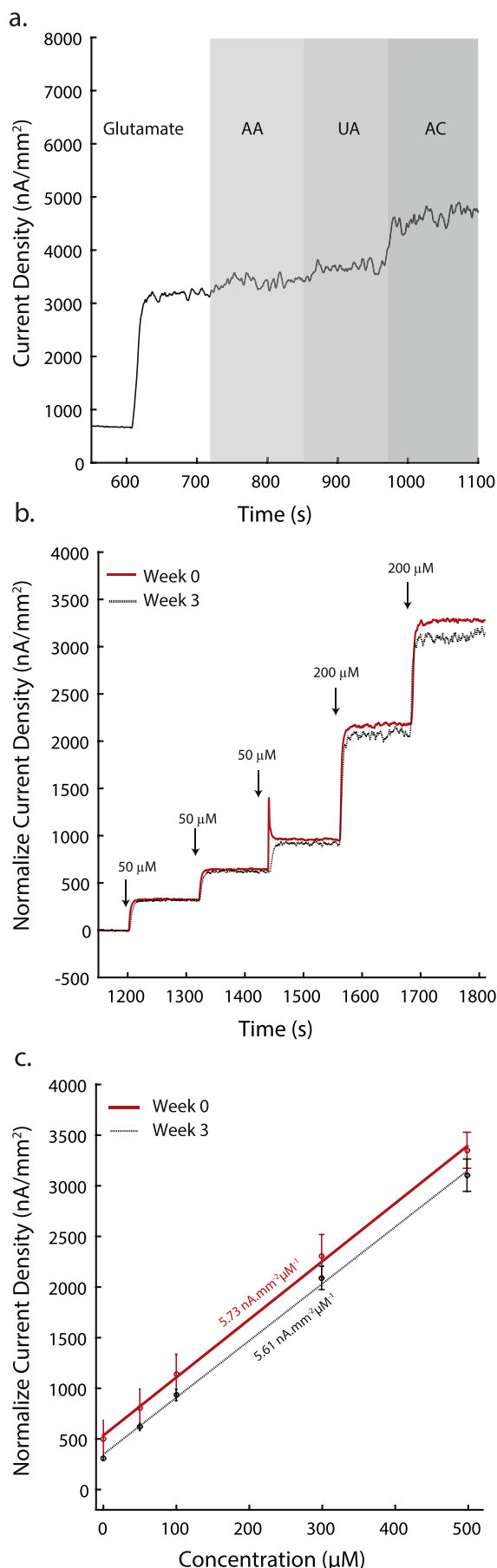
sensitivity of these rapid prototyped biosensors using CPt matrix with higher Pt composition (*i.e.*, >1%).

3.4. Biosensor specificity and stability

Although enzymes are well-known for their specificity, oxidase biosensors are often affected by non-specific signals from electroactive species present in the milieu. For example, ascorbic acid (AA), uric acid (UA), acetaminophen (AC), 3,4-Dihydroxyphenylacetic acid (DOPAC), and 5-hydroxyindoleacetic acid (5-HIAA) are often found in the body, and they can be oxidized at the electrode surface. To improve our biosensor specificity, we used Nafion as a permselective membrane. Fig. 6a shows that our biosensor can effectively block signals from AA (100 μM) and UA (100 μM) without affecting glutamate sensitivity. However, we were not able to block the signal from AC (100 μM). We were only able to block signals from DOPAC and 5-HIAA using annealed Nafion but the sensitivity of the biosensor decreased (Fig. S8). We may be able to better address these sources of noise by using a different permselective membrane such as o-aminophenol, *m*-phenylenediamine dihydrochloride [36,37].

We also measured the stability of our glutamate biosensors by quantifying the change in their sensitivities before and after storage at 4 °C in 0.01 M PBS (pH 7.0) for 3 weeks. The *i-t* responses and calibration curves of our glutamate biosensors before and after the storage period were presented in Fig. 6b and c. When the sensors were refrigerated, they retained 97.9% of their initial sensitivities ($n = 3$). We also characterized the reusability of our glutamate biosensor by quantifying the change in their sensitivities before and after bending 100–1000 times (Fig. S6). After bending 100 times, the sensitivity changed ~2.5% compare to the original value ($n = 3$). After a 1000 bend cycles, the sensitivity changed ~6% ($n = 3$). Finally, we repeated the amperometric measurements of the same device multiple times to gauge its durability ($n = 3$). We found that repeated testing of each device showed ~3% change in sensitivity between the first and eighth run (Fig. S7 and Table S3).

3.5. Measuring glutamate uptake from astrocytes

To further demonstrate the sensor functionality, we measured the changes in glutamate concentration using primary human astrocyte culture. Fig. 7a shows our printed glutamate biosensor in astrocyte culture ~100 μM away. When a bolus of glutamate (225 μM) is added, the biosensor responded rapidly with a current spike, which ultimately settled around 10 min (Fig. 7b). The glutamate concentration was estimated to be about 125 μM after 10 min in astrocyte culture, which is likely due to glutamate consumption by astrocytes (Fig. 7c) at the density of electrode surface. Measurements from the astrocytes had greater standard deviation than the control, which may be due to different levels of cell density at the time of experiment.

One of the limitations of using a single channel biosensor is that it is not possible to ascertain concentration gradient of the analyte. We may be able to further elucidate on the characteristics of astrocyte-mediated glutamate concentration gradient by printing a linear array of glutamate biosensors and measuring at specific distances simultaneously. The measurement from biosensor array may be useful for quantifying the relationship between the glutamate concentration at the cell surface and the glutamate uptake rate [14,38,39].

Fig. 6. (a) A response of C-Pt–PEDOT:PSS composite upon sequential addition of 200 μM glutamate, 100 μM of AA, 100 μM of UA and 100 μM of AC into constantly stirred 0.01 M PBS (pH 7.0) solution. (b) An amperometric response of different concentrations of glutamate in 0.01 M PBS solution (pH 7.0) of C-Pt–PEDOT:PSS composite before and after 3 weeks of storage ($n = 3$). (c) The corresponding calibration curve and sensitivity of C-Pt–PEDOT:PSS composite before and after 3 weeks of storage ($n = 3$).
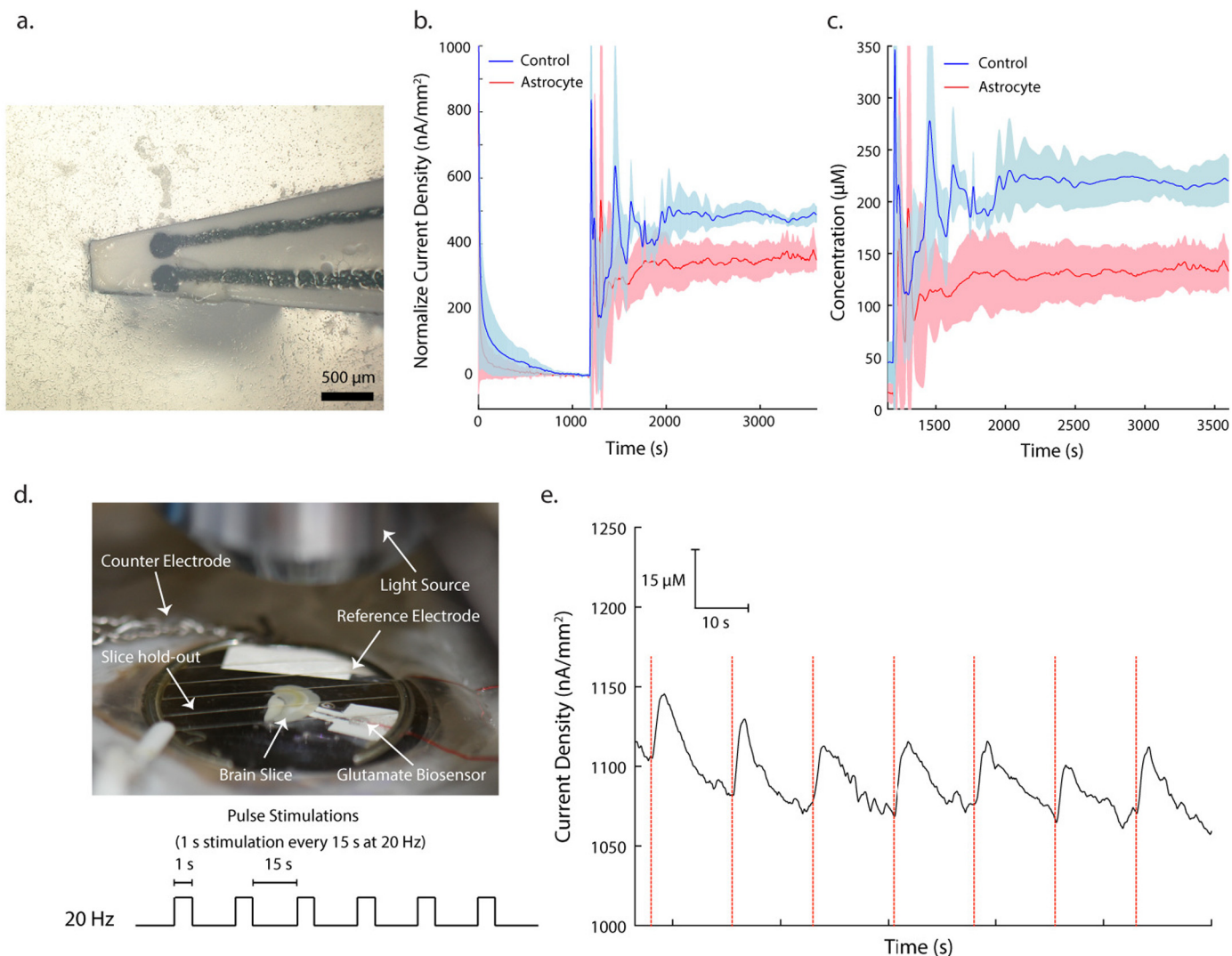
Fig. 7. (a) A photograph of glutamate biosensor (foreground) over an astrocyte cell culture (background). (b) Measurement of glutamate consumption by astrocyte cells. Blue: mean current response 100 μm from the surface of culture well following addition of 225 μM glutamate without astrocytes (control, $n = 3$). The blue shading indicates the standard deviation of the three samples. Red: mean current response 100 μm from the surface of culture well following addition of 225 μM glutamate into the astrocyte cell culture. The red shading indicates the standard deviation of three measurements with astrocytes. (c) Estimated glutamate concentration during the glutamate consumption experiments with and without astrocytes. (d). Optogenetic-induced glutamate release setup using a visual cortex brain slice from a mouse (top). Train laser pulse stimulations for 1 s, which were delivered at 20 Hz every 15 s (bottom). (e) Representative of an *ex vivo* light-induced glutamate sensing curve. The dashed red lines indicated the time when stimulations were applied.

3.6. Measuring glutamate release from mouse visual cortex by optogenetic stimulation

To further demonstrate the potential use of these biosensors for real-time biological applications, we measured glutamate from optogenetic-induced release in mouse brain slices. Working electrodes were calibrated before and after tissue experiments. Extracellular glutamate changes were quantified during light activation of visual cortex in mice. Light pulses of 5 ms width were applied as described in Methods section (Fig. 7d), 1 s duration every 15 s at 20 Hz. Fig. 7e shows a representative of precise optical control of glutamate release. There was a pronounced increase in peak current density right after the stimulation. Furthermore, the temporal dynamics of glutamate release in this stimulation was very robust with <1 s after each stimulation. The dashed red lines in Fig. 7e indicated where stimulations were applied. The peak current density per mm^2 was averaged over 40 trials of light stimulation in three samples, indicating average concentration recorded per stimulation was 11.43 ± 2.00 μM ($n = 3$). The results

suggest that the ChR2-control of glutamate release was robust and can be successfully measured by using the CPt glutamate biosensor.

4. Conclusion

In this work, we presented a simple manufacturing technique for creating a highly sensitivity glutamate biosensors using low-cost C-Pt–PEDOT:PSS composite ink. The biosensor can be rapidly prototyped using DIW on various substrate. The printed biosensors performed better than MEMS-fabricated and Pt nanoparticle-based glutamate biosensors in terms of their sensitivity. The sensor had high sensitivity of 5.73 ± 0.08 nA μM^{-1} mm^{-2}, a good linear range from 1 μM up to 925 μM (R^2 = 0.996), a low detection limit of with 0.03 μM, and a fast response time ≤ 1 s. Furthermore, our sensor demonstrated good specificity for glutamate when tested against AA and UA. Additional work is needed to optimize permselective layer to prevent oxidation of AC, DOPAC, 5-HIAA. In the future, we plan to perform additional

experiments to better quantify the dynamic extracellular glutamate concentration in various *in vitro* and *in vivo* models. Furthermore, we plan to apply the similar fabrication techniques for other sensing applications using different recognition elements.

CRediT authorship contribution statement

Tran N.H. Nguyen: Conceptualization, Methodology, Investigation, Validation, Visualization, Writing-original draft, Writing-review & editing.**James Nolan:**Investigation, Writing-original draft, Writing-review & editing.**Xi Cheng:**Investigation, Writing-reviewer & editing.**Hyunsu Park:**Investigation, Resources.**Yi Wang:**Investigation.**Stephanie Lam:**Investigation.**Hyungwoo Lee:**Formal analysis, Resources.**Sang Joon Kim:** Formal analysis, Resources.**Riyi Shi:**Conceptualization, Resources.**Alexander A. Chubykin:**Conceptualization, Methodology, Supervision, Writing-reviewer & editing.**Hyowon Lee:**Conceptualization, Methodology, Formal analysis, Supervision, Funding acquisition, Writing-original draft, Writing-review & editing.

Declaration of competing interest

The authors declare that they have no known competing financial interests or personal relationships that could have appeared to influence the work reported in this paper.

Acknowledgment

Appendix A. Supplementary data

Supplementary data to this article can be found online at https://doi.org/10.1016/j.jelechem.2020.114136.

References

[1] A. Barria, D. Muller, V. Derkach, L.C. Griffith, T.R. Soderling, Regulatory phosphorylation of AMPA-type glutamate receptors by CaM-KII during long-term potentiation, Science 276 (5321) (1997) 2042–2045.

[2] L. Hertz, Glutamate, a neurotransmitter-and so much more. A synopsis of Wierzba III, Neurochem. Int. 48 (6–7) (2006) 416–425.

[3] A. Doble, The role of excitotoxicity in neurodegenerative disease: implications for therapy, Pharmacol. Ther. 81 (3) (1999) 163–221.

[4] D. Nicholls, D. Attwell, The release and uptake of excitatory amino acids, Trends Pharmacol. Sci. 11 (11) (1990) 462–468.

[5] J.A. Dzubay, C.E. Jahr, The concentration of synaptically released glutamate outside of the climbing fiber-Purkinje cell synaptic cleft, J. Neurosci. 19 (13) (1999) 5265–5274.

[6] G.Y. Xu, M.G. Hughes, Z. Ye, C.E. Hulsebosch, D.J. McAdoo, Concentrations of glutamate released following spinal cord injury kill oligodendrocytes in the spinal cord, Exp. Neurol. 187 (2) (2004) 329–336.

[7] A. Weltin, J. Kieninger, G.A. Urban, Microfabricated, amperometric, enzyme-based biosensors for in vivo applications, Anal. Bioanal. Chem. 408 (17) (2016) 4503–4521.

[8] L. Pellerin, P.J. Magistretti, Neuroenergetics: calling upon astrocytes to satisfy hungry neurons, Neuroscientist 10 (1) (2004) 53–62.

[9] J.J. Burmeister, G.A. Gerhardt, Self-referencing ceramic-based multisite microelectrodes for the detection and elimination of interferences from the measurement of L-glutamate and other analytes, Anal. Chem. 73 (5) (2001) 1037–1042.

[10] E.C. Rutherford, F. Pomerleau, P. Huettl, I. Strömberg, G.A. Gerhardt, Chronic second-by-second measures of L-glutamate in the central nervous system of freely moving rats, J. Neurochem. 102 (3) (2007) 712–722.

[11] C.P. McMahon, R.D. O'Neill, Polymer-enzyme composite biosensor with high glutamate sensitivity and low oxygen dependence, Anal. Chem. 77 (4) (2005) 1196–1199.

[12] N. Hamdi, J. Wang, E. Walker, N.T. Maidment, H.G. Monbouquette, An electroenzymatic l-glutamate microbiosensor selective against dopamine, J. Electroanal. Chem. 591 (1) (2006) 33–40.

[13] Y. Cui, J.P. Barford, R. Renneberg, Development of an interference-free biosensor for l-glutamate using a bienzyme salicylate hydroxylase/l-glutamate dehydrogenase system, Enzym. Microb. Technol. 41 (6–7) (2007) 689–693.

[14] E.S. McLamore, S. Mohanty, J. Shi, J. Claussen, S.S. Jedlicka, J.L. Rickus, D.M. Porterfield, A self-referencing glutamate biosensor for measuring real time neuronal glutamate flux, J. Neurosci. Methods 189 (1) (2010) 14–22.

[15] L.N.Q. Hoa, H.R. Chen, T.T. Tseng, An arrayed micro-glutamate sensor probe integrated with on-probe Ag/AgCl reference and counter electrodes, Electroanalysis 30 (3) (2018) 561–570.

[16] J.L. Scoggin, C. Tan, N.H. Nguyen, U. Kansakar, M. Madadi, S. Siddiqui, P.U. Arumugam, M.A. DeCoster, T.A. Murray, An enzyme-based electrochemical biosensor probe with sensitivity to detect astrocytic versus glioma uptake of glutamate in real time in vitro, Biosens. Bioelectron. 126 (2019) 751–757.

[17] J.A. Lewis, Direct ink writing of 3D functional materials, Adv. Funct. Mater. 16 (17) (2006) 2193–2204.

[18] T.N. Nguyen, J.K. Nolan, H. Park, S. Lam, M. Fattah, J.C. Page, H.E. Joe, M.B. Jun, H. Lee, S.J. Kim, R. Shi, H. Lee, Facile fabrication of flexible glutamate biosensor using direct writing of platinum nanoparticle-based nanocomposite ink, Biosens. Bioelectron. 131 (2019) 257–266.

[19] T.N. Nguyen, S. Lam, H. Park, R. Shi, H. Lee, Development of flexible glutamate biosensor using activated carbon - Pt microparticle composite ink, Proceedings of IEEE Sensors, Vol. 2018-Octob, 2018.

[20] J. Park, A. Lee, Y. Yim, E. Han, Electrical and thermal properties of PEDOT:PSS films doped with carbon nanotubes, Synth. Met. 161 (5–6) (2011) 523–527.

[21] A.J. Bandodkar, R. Nuñez-Flores, W. Jia, J. Wang, All-printed stretchable electrochemical devices, Adv. Mater. 27 (19) (2015) 3060–3065.

[22] Q. Wu, I. Kolb, B.M. Callahan, Z. Su, W. Stoy, S.B. Kodandaramaiah, R. Neve, H. Zeng, E.S. Boyden, C.R. Forest, A.A. Chubykin, Integration of autopatching with automated pipette and cell detection in vitro, J. Neurophysiol. 116 (4) (2016) 1564–1578.

[23] B.R. Arenkiel, J. Peca, I.G. Davison, C. Feliciano, K. Deisseroth, G.J. Augustine, M.D. Ehlers, G. Feng, In vivo light-induced activation of neural circuitry in transgenic mice expressing channelrhodopsin-2, Neuron 54 (2) (2007) 205–218.

[24] G. Yang, K.L. Kampstra, M.R. Abidian, High-performance conducting polymer nanofiber biosensors for detection of biomolecules, Adv. Mater. 26 (29) (2014) 4954–4960.

[25] L. Kergoat, B. Piro, D.T. Simon, M.C. Pham, V. Noël, M. Berggren, Detection of glutamate and acetylcholine with organic electrochemical transistors based on conducting polymer/platinum nanoparticle composites, Adv. Mater. 26 (32) (2014) 5658–5664.

[26] S. Govindarajan, C.J. McNeil, J.P. Lowry, C.P. McMahon, R.D. O'Neill, Highly selective and stable microdisc biosensors for l-glutamate monitoring, Sensors Actuators B Chem. 178 (2013) 606–614.

[27] S. Biniak, A. Swiatkowski, M. Pakuta, Electrochemical studies of phenomena at active carbon-electrolyte solution interfaces, Chemistry & Physics of Carbon 2001, pp. 125–225.

[28] Harry Marsh, F. Rodrguez-Reinoso, CHAPTER 4 - characterization of activated carbon, Activated Carbon (2006) 143–242.

[29] A. Bach, R. Semiat, The role of activated carbon as a catalyst in GAC/iron oxide/H_2O_2 oxidation process, Desalination 273 (1) (2011) 57–63.

[30] S. Venkatraman, J. Hendricks, Z.A. King, A.J. Sereno, S. Richardson-Burns, D. Martin, J.M. Carmena, In vitro and in vivo evaluation of PEDOT microelectrodes for neural stimulation and recording, IEEE Transactions on Neural Systems and Rehabilitation Engineering 19 (3) (2011) 307–316.

[31] H.H. Hsieh, F.C. Hsu, Y.F. Chen, Energetically autonomous, wearable, and multifunctional sensor, ACS Sensors 3 (1) (2018) 113–120.

[32] S.C. Perry, S.M. Gateman, J. Sifakis, L. Pollegioni, J. Mauzeroll, Enhancement of the enzymatic biosensor response through targeted electrode surface roughness, J. Electrochem. Soc. 165 (12) (2018) G3074–G3079.

[33] R. Gerwig, K. Fuchsberger, B. Schroeppel, G. S. Link, G. Heusel, U. Kraushaar, W. Schuhmann, A. Stett, M. Stelzle, PEDOT–CNT composite microelectrodes for recording and electrostimulation applications: fabrication, morphology, and electrical properties, Frontiers in Neuroengineering 5.

[34] S. Hrapovic, Y. Liu, K.B. Male, J.H. Luong, Electrochemical biosensing platforms using platinum nanoparticles and carbon nanotubes, Anal. Chem. 76 (4) (2004) 1083–1088.

[35] D. Wen, X. Zou, Y. Liu, L. Shang, S. Dong, Nanocomposite based on depositing platinum nanostructure onto carbon nanotubes through a one-pot, facile synthesis method for amperometric sensing, Talanta 79 (5) (2009) 1233–1237.

[36] M.L. Stephens, J.E. Quintero, F. Pomerleau, P. Huettl, G.A. Gerhardt, Age-related changes in glutamate release in the CA3 and dentate gyrus of the rat hippocampus, Neurobiol. Aging 32 (5) (2011) 811–820.

[37] A. Weltin, J. Kieninger, B. Enderle, A.K. Gellner, B. Fritsch, G.A. Urban, Polymer-based, flexible glutamate and lactate microsensors for in vivo applications, Biosens. Bioelectron. 61 (2014) 192–199.

[38] J.F. Rivera, S.V. Sridharan, J.K. Nolan, S.A. Miloro, M.A. Alam, J.L. Rickus, D.B. Janes, Real-time characterization of uptake kinetics of glioblastoma: vs. astrocytes in 2D cell culture using microelectrode array, Analyst 143 (20) (2018) 4954–4966.

[39] S.V. Sridharan, J.F. Rivera, J.K. Nolan, M.A. Alam, J.L. Rickus, D.B. Janes, On-chip microelectrode array and in situ transient calibration for measurement of transient concentration gradients near surfaces of 2D cell cultures, Sensors Actuators B Chem. 260 (2018) 519–528.

[40] M. van der Zeyden, W.H. Oldenziel, K. Rea, T.I. Cremers, B.H. Westerink, Microdialysis of GABA and glutamate: analysis, interpretation and comparison with microsensors, Pharmacol. Biochem. Behav. 90 (2) (2008) 135–147.

[41] V.H. Cifuentes Castro, C.L. López Valenzuela, J.C. Salazar Sánchez, K.P. Peña, S.J. López Pérez, J.O. Ibarra, A.M. Villagrán, An update of the classical and novel methods used for measuring fast neurotransmitters during normal and brain altered function, Curr. Neuropharmacol. 12 (6) (2014) 490–508.

[42] S. Ramadan, A. Lin, P. Stanwell, Glutamate and glutamine: a review of in vivo MRS in the human brain, NMR Biomed. 26 (12) (2013) 1630–1646.

[43] K.L. Behar, D.L. Rothman, In vivo nuclear magnetic resonance studies of glutamate-γ-aminobutyric acid-glutamine cycling in rodent and human cortex: the central role of glutamine, J. Nutr. 131 (9) (2001) 2498S–2504S.

[44] G. Muehllehner, J.S. Karp, Positron emission tomography, Phys. Med. Biol. 51 (13) (2006) R117–37.

[45] M. Kagedal, Z. Cselenyi, S. Nyberg, P. Raboisson, L. Stahle, P. Stenkrona, K. Varns, C. Halldin, A.C. Hooker, M.O. Karlsson, A positron emission tomography study in healthy volunteers to estimate mGluR5 receptor occupancy of AZD2066 - estimating occupancy in the absence of a reference region, NeuroImage 82 (2013) 160–169.

[46] J.P. Issberner, C.L. Schauer, B.A. Trimmer, D.R. Walt, Combined imaging and chemical sensing of L-glutamate release from the foregut plexus of the Lepidopteran, Manduca sexta, J. Neurosci. Methods 120 (1) (2002) 1–10.

[47] M. Pospíšilová, G. Kuncová, J. Trögl, Fiber-optic chemical sensors and fiber-optic biosensors, Sensors 15 (10) (2015) 25208–25259.

[48] P. Salazar, M. Martín, R.D. O'Neill, J.L. González-Mora, Glutamate microbiosensors based on Prussian Blue modified carbon fiber electrodes for neuroscience applications: in-vitro characterization, Sensors Actuators B Chem. 235 (2016) 117–125.

[49] T.T.C. Tseng, H.G. Monbouquette, Implantable microprobe with arrayed microsensors for combined amperometric monitoring of the neurotransmitters, glutamate and dopamine, J. Electroanal. Chem. 682 (2012) 141–146.

[50] M. Zhang, C. Mullens, W. Gorski, Amperometric glutamate biosensor based on chitosan enzyme film, Electrochim. Acta 51 (21) (2006) 4528–4532.

[51] M. Ammam, J. Fransaer, Highly sensitive and selective glutamate microbiosensor based on cast polyurethane/AC-electrophoresis deposited multiwalled carbon nanotubes and then glutamate oxidase/electrosynthesized polypyrrole/Pt electrode, Biosens. Bioelectron. 25 (7) (2010) 1597–1602.

[52] R. Khan, W. Gorski, C.D. Garcia, Nanomolar detection of glutamate at a biosensor based on screen-printed electrodes modified with carbon nanotubes, Electroanalysis 23 (10) (2011) 2357–2363.